HHS Public Access

Author manuscript

J Mater Chem B Mater Biol Med. Author manuscript; available in PMC 2016 November 14.

Published in final edited form as:

J Mater Chem B Mater Biol Med. 2015 November 14; 3(42): 8314–8320. doi:10.1039/C5TB01692D.

Design of Silk-Vaterite Microsphere Systems as Drug Carriers with pH-responsive Release Behavior

S. S. Liu[a,b], **L. J. Liu**[a,b], **L. Y. Xiao**[a,b], **Q. Lu**[a,b,*], **H. S. Zhu**[c], and **D. L. Kaplan**[a,d]

[a]National Engineering Laboratory for Modern Silk & Collaborative Innovation Center of Suzhou Nano Science and Technology, Soochow University, Suzhou 215123, People's Republic of China

[b]College of Textile and Clothing Engineering, Soochow University, Suzhou 215123, People's Republic of China

[c]Research Center of Materials Science, Beijing Institute of Technology, Beijing 100081, People's Republic of China

[d]Department of Biomedical Engineering, Tufts University, Medford, MA02155, USA

Abstract

Improving the therapeutic efficacy of chemotherapy remains a key goal for cancer therapy. Various passive and active targeting strategies have been developed to facilitate drug release targeted to cancer lesions, but actively designing tunable drug release behavior for these needs remains a challenge. As a step towards this need, silk-vaterite microspheres were fabricated and utilized as carriers to tune drug release. Doxorubicin (DOX) was loaded on the microspheres with high efficiency and the release behavior was regulated by tuning the microspheres via thermal processing. *In vitro* cell inhibition results showed that the drug-loaded microspheres had different cytotoxic efficiencies depending on the DOX release rates. Better efficacy at lower drug doses suggests options to optimize anticancer effects while minimizing toxic side effects. The tunable drug release capacity combined with the inherent passive targeting property of vaterite-based carriers based on pH sensitivity suggests a promising system for enhanced efficacy of chemotherapy.

Introduction

Chemotherapy is a general approach for the treatment of cancers, but in many instances has limited therapeutic effect due to serious side effects and a lack of tumor selectivity[1–4]. In order to improve chemotherapy, various systems (DDSs) have been developed to control the delivery of anticancer drugs such as doxorubicin (DOX)[5–13]. Although various targeting agents have been introduced to DDSs to improve dosing to tumors, most targeted DDSs are polymer-based carrier designs with limitations due to complex synthesis procedures and safety concerns[14–19]. Therefore, designing biocompatible and targeted DDS via facile preparation processes is of significant interest.

*Corresponding author, Tel: (+86)-512-67061649; lvqiang78@suda.edu.cn.

Electronic Supplementary Information (ESI) available: [details of any supplementary information available should be included here]. See DOI: 10.1039/x0xx00000x

Unlike polymers, inorganic materials are usually prepared through relatively mild preparation processes without the need for toxic reagents[20–25]. Porous $CaCO_3$ materials can be loaded with anticancer drugs and are also biocompatible and biodegradable[26–36]. The natural pH-sensitive structure of this inorganic material endows targeting capacity for drug release within tumors due to the more rapid degradation of the system in the acidic tumors environment. These materials can also enhance cytotoxicity against cancer cells by increasing cellular uptake, perinuclear accumulation, and nuclear entry. $CaCO_3$ encapsulation of functional agents such as Au-DNA and Fe_3O_4 nanoparticles has been proposed to generate combined photothermal and chemotherapy systems[22]. However, these DDSs usually require sophisticated designs and engineering, resulting in significant limitations for clinical translation[34, 37–38]. Although both active and passive targeting properties are achieved for $CaCO_3$ carriers, challenges remain to actively control drug release behavior around cancerous tissue to enhance the anticancer effect of drugs[39–41]. The development of novel $CaCO_3$ DDS with improved therapeutic performance along with simplified preparation remains a need.

Silk fibroin has been used to regulate calcium carbonate polymorphy and morphologies in mineralization process.[42–44] Inspired by these studies, we recently introduced silk fibroin in calcium carbonate biomineralization processes, resulting in the formation of highly uniform vaterite microspheres[45]. The microspheres, as drug carriers of DOX, have good encapsulation efficiency, sustained drug release without burst release, and pH sensitivity. Unlike vaterite systems reported previously[46–51], the present vaterite microspheres have sufficient stability in aqueous solution without transformation into calcite, due to the existence of the silk matrix as a templating moiety. Considering the critical influence of silk on maintaining the stability of vaterite, we hypothesized that the stability of the vaterite microspheres could be regulated further by tuning the content of the embedded silk fibroin, achieving control of drug release behavior.

Here, we demonstrated thermal treatment for the generation of vaterite carrier systems with tunable stability, achieved through control of the silk structure in the microspheres. These silk-vaterite microspheres were prepared according to our previously reported procedure[45]. The microspheres were then treated at different temperatures for various times to partly decompose the silk where the temperature was below the crystallization transition temperature, avoiding calcite formation. After the thermal treatment, the vaterite microspheres could have various stabilities, which further resulted in corresponding different drug release behaviors, suggesting utility as drug carriers.

Material and Methods

Materials

Analytical grade calcium chloride ($CaCl_2$) and ammonium bicarbonate (NH_4HCO_3) (Sinopharm Chemical Reagent Co. Ltd., Beijing, China) were used without further purification. Doxorubicin Hydrochloride (DOX) was purchased from Beijing Huafeng United Technology CO., Ltd., China. All glasses were cleaned and sonicated in ethanol for 10 min, further soaked with a H_2O-HNO_3 (65%)-H_2O_2 (1:1:1 by volume) solution, and then rinsed with deionized water and dried in air.

Preparation of silk solution

Silk solutions were prepared according to our previously established procedures[52]. *Bombyx mori* silk fibers were boiled for 20 min in an aqueous solution of 0.02 M Na_2CO_3, and then rinsed thoroughly with distilled water to extract the sericin proteins. Then the extracted silk was dissolved in 9.3 M LiBr solution at 60 °C for 4 h, yielding a 20 (w/v) % solution. The solution was dialyzed against distilled water using a dialysis tube (Pierce, molecular weight cut-off 3,500) for 3 days to remove the salt. The dialyzed solution was centrifuged at 9,000 rpm for 20 min to remove silk aggregates and other impurities formed during the process. The concentration of aqueous silk solution was about 7 wt%, determined by weighing the remaining solid after drying. The fresh solution was then cultured at 60 °C for 24 h to induce nanoparticle formation based on our recent study[53].

Preparation of silk-vaterite microspheres

Silk-vaterite microspheres were prepared according to our previously published procedure[45]. An aqueous solution of $CaCl_2$ (0.27 mol/L, 5 mL) was added into aqueous silk solution (4 wt%, 15 mL), and kept quiescent for 30 min. Then NH_4HCO_3 solution (0.54 mol/L, 5 mL) was injected into the blend system under vigorous stirring at 700 rpm. After stirring for 10 min, the solution was allowed to stand for 1 h at room temperature. Silk-vaterite microspheres were obtained by centrifuging the experiential suspension and washing three times with deionized water, and then dried at room temperature for further characterization.

Thermal treatment of the silk-vaterite microspheres

As shown in Scheme 1, the silk-vaterite microspheres were treated at different temperatures to partly decompose the silk. Based on serial thermal treatment processes, it was found that the microspheres were placed at 300 °C, 305 °C and 310 °C for 10 min, 2 hours and 6 hours, respectively, to form silk-vaterite microspheres with significant different silk contents and also different stabilities. Therefore, the silk-vaterite microspheres were treated under the above conditions and the thermally treated microspheres were termed M-300, M-305 and M-310, respectively.

Characterization

The morphologies of the microsphere samples were characterized with scanning electron microscopy (SEM, S-4800, Hitachi, Tokyo, Japan). The samples were sputter coated with platinum and then measured with SEM at 3 kV. The polymorph of the vaterite samples was assessed with X-ray diffraction (XRD). The XRD measurement was conducted with an X-ray diffractometer (X'Pert-Pro MPD, PANalytical, Almelo, Holland) with Cu Kα radiation at 40 kV and 30 mA and scanning rate of 0.6 °/min. Fourier transform infrared spectroscopy (FTIR) was carried out with a Nicolet FTIR 5700 spectrometer (Thermo Scientific, Florida, USA) in the range 4000-400 cm^{-1} to determine the presence of silk in the vaterite microspheres. N_2 gas sorption isotherms were obtained using an ASAP 2020 instrument (Micromeritics, GA, USA). Specific surface areas and pore size distributions were derived from the isotherms using BET calculations.

Loading and release of DOX in the silk-vaterite microspheres

Twenty milligrams of microspheres were added into 2 mL DOX aqueous solution (0.5 mg/mL). The mixture was shaken in the thermostatic shaker for 24 h at room temperature. Then, the products were collected by centrifugation at 6,000 rpm for 10 min, washed twice with 1 mL deionized water and dried for future use. The DOX content of the supernatant was determined by measuring the absorbance at 486 nm with a microplate reader (Synergy H1, BioTek, Vermont, USA) based a calibration curve. The loading content and entrapment efficiency of DOX was calculated as follows.

$$\text{Drug loading content} = (W_T - W_F)/W_{CM} \times 100\%$$

$$\text{Entrapment efficiency} = (W_T - W_F)/W_T \times 100\%$$

Where W_T is the total weight of DOX in the reaction, W_F is the total weight of free DOX remaining in the supernatant, and W_{CM} is the total weight of the $CaCO_3$ microspheres loaded with DOX. The data are presented as mean ± standard deviation (SD) based on the triplicate measurements of the different samples.

For drug release studies, twenty milligrams of the dried DOX-loaded microspheres after washing treatment were added into 2 mL PBS solution at different pH values (4.5 and 7.4) and placed in a thermostatic shaker at 37 °C. At predetermined intervals, 1 mL of the supernatant was taken and analyzed by measuring the absorbance at 486 nm. The same volume (1 mL) of fresh PBS buffer at different pH values were added into the release medium. The release behaviors over time were based on one sample and the release measurements were repeated in triplicate from different samples.

Cellular experiments

Human breast cancer cells (MDA-MB-231), obtained from Cell Bank of Chinese Academy of Sciences, were cultured with DOX-free silk-vaterite microspheres (M-0), Free DOX, DOX-loaded M-0, DOX-loaded M-300, DOX-loaded M-305 and DOX-loaded M-310 with various DOX concentrations to assess the influence of the drug release on cancer cells, respectively. The MDA-M-231 human breast cancer cells were pre-seeded in 96-well plates at 5×10^3 cells/well were incubated with different concentrations of DOX-loaded vaterite or free DOX for 5 days. The standard cell viability CCK-8 assay was carried out to determine cell viabilities relative to the untreated control.

Statistics

All statistical analyses were performed using SPSS v.16.0 software. Comparison of the mean values of the data sets was performed using Student-Newman-Keuls test. Measures are presented as means ± standard deviation, unless otherwise specified. $P < 0.05$ was considered significant.

Results and Discussion

The strategy for the thermal treatment of silk-vaterite microspheres was shown in Scheme 1. Recent studies have indicated that silk could be removed without impacting a transition from vaterite to calcite when the microspheres were treated at 310 °C[45, 54]. Therefore, the

microspheres were treated at 300 °C, 305 °C and 310 °C for 10 min, 2 h and 6 h, respectively, to partially remove silk. These microspheres were termed M-300, M-305 and M-310, respectively, while the microspheres without the thermal treatment were designated M-0. The weight losses due to the treatments were 87%, 85% and 81%, corresponding to silk removal of 20%, 40% and 95%, respectively (Figure 1). FTIR spectra indicated that the intensity of silk bands (1500–1600 cm^{-1}) gradually decreased following the increase in thermal treatment temperature and time, and almost disappeared when the microspheres were treated at 310 °C for 6 h, confirming the removal of silk. The constancy of typical vaterite bands (1082, 870 and 750 cm^{-1}) after the various treatments indicated the stability of the vaterite state, which was further confirmed with XRD curves.

After the thermal treatments, the silk-vaterite materials remained intact, but had a rougher surface with more voids due to the removal of silk (Figure 2). Cross-section images of the microspheres showed that they were composed of vaterite nanoparticles with size of about ten nanometers. The removal of silk resulted in more voids within the microspheres, and the vaterite nanoparticles inside the microspheres began to fuse at the higher temperatures. It was found that the nanoparticles inside the microspheres maintained unchangeable when treated at 300 °C and 305 °C and then began to fuse after treated at 310 °C (Figure 2d Insert). Further treatment at higher temperature (350°C) could confirm this tendency as the microspheres became smooth with the larger fused particle formation inside (Figure S1). The micro-structural changes of the microspheres also resulted in changes in surface area (Figure S2). The surface area of the microspheres increased from 54.5 to 72.5 m^2/g after the treatment at 300 °C because of the loss of silk, while the surface area of the microspheres decreased to 8.9 m^2/g when the treatment temperature was 310 °C, possibly due to the fusion of the nanoparticles. Therefore, when treated at a designed temperature, tunable silk content and surface features could be achieved without the loss of the vaterite structure. The microspheres were incubated in flowing water to assess stability. Different crystal transition processes were found in the microspheres with the various silk contents (Figure 3, 4). Vaterite to calcite transformation occurred in treated microspheres after incubation for 8 days in the flowing water, revealing the metastable state of the inorganic phase. After incubation for 2 days, the M-0 and M-300 microspheres kept stable without the vaterite-calcite transformation while partly transformation happened in the M-305 microspheres and most of vaterite has been transformed into calcite inside the M-310 microspheres. After 4 days, the vaterite inside the M-305 microspheres has almost disappeared and the transformation from vaterite to calcite appeared in the M-300 microspheres. After incubation for 8 days, the transformation inside the M-300 microspheres became significant, but the microspheres without thermal treatment still remained spherical with typical vaterite peaks. Therefore, as expected, these microspheres had different transformation rates where the significant transformation from vaterite to calcite appeared after 2, 4 and 8 days for M-310, M-305 and M-300, respectively. More elaborate stability control of silk-vaterite is expected through further regulating thermal treatment conditions to achieve desired drug delivery.

Various studies have suggested the critical function of vaterite stability in regulating drug release[28–29]. The thermally treated microspheres exhibited silk content-dependent stability in aqueous solution, allowing them to be studied as drug release materials with designed

release behaviors. DOX was used as a model drug to study release. The ratio of drug and vaterite was fixed to 1:20 (w/w) based on a previous study[45]. Absorbance analysis showed that the entrapment efficiency of DOX was above 90% for all the microspheres (Table 1), significantly higher than previous results with submicrometer vaterite carriers[46–51]. Similar to some mesoporous calcium phosphate microspheres with different surface areas[55], the silk-vaterite microspheres with different surface areas and silk contents after thermal treatment showed similar entrapment efficiency. The results suggested that the drug absorption might be depended on the hydrophobic interactions between the drug and vaterite/carbonized ingredients derived from the decomposed silk, rather than the voids of vaterite. Further insight into the loading mechanism will be needed to clarify the relationships. However, it is worth noting that the similar loading capacity of the different thermally treated microspheres is pivotal to the success of DDS design to avoid variations in drug loading.

We next clarified whether the drug release of DOX loaded microspheres could be tuned by regulating the stability of the microspheres. The different microspheres (M-0, M-300, M-305 and M-310) with the same DOX content were incubated in PBS at pH 7.4 and 4.5, respectively. The cumulative release of DOX was measured at various time points (Figure 5), showing pH dependent release behavior that was significantly higher at pH 4.5 than at pH 7.4. After 8 days, the amount of DOX released at pH 7.4 was below 16% for all the samples while the amount of DOX released at pH 4.5 reached 76%, 57%, 38% and 26% of the total drug load for M-0, M-300, M-305 and M-310, respectively, which suggested a reverse relationship between drug release and microsphere stability. This finding was reasonable since metastable vaterite could transform into stable calcite/hydroxyapatite more quickly to form a coating to restrain drug release (Figures 3, 4, S3). Further control of the release behavior was achieved by blending different DOX-loaded microspheres at designed ratios (Figure 5 c, d). When the ratio of two different DOX-loaded microspheres was kept at 1:1 (w/w), the carrier composed of two different microspheres showed an intermediary release rate compared to that of the single microsphere carrier, which reached 62%, 42%, 26% after 8 days, respectively. The release rate of composite drug-loaded microspheres (M-305 and M-310) was similar to that of drug-loaded M-310 microspheres while the drug release rate of the two other composite carriers was below the mean value of the corresponding two carriers, suggesting that there was no linear relation between the release behavior and the ratios of different microsphere carriers. Further studies are necessary to clarify the influence of carrier composition on drug release behaviors. However, besides pH response, these *in vitro* drug release results indicated that drug release behavior could be tuned and designed via the above processes, useful for improving therapeutic efficacy in chemotherapy.

The influence of different drug release behaviors on cancer cells was studied *in vitro*. Human breast cancer cells (MDA-MB-231) were incubated with DOX-free vaterite microspheres (M-0), Free DOX, DOX-loaded M-0, DOX-loaded M-300, DOX-loaded M-305 and DOX-loaded M-310 for 5 days. The relative cell viabilities were determined by CCK-8 assay. As expected, both free and loaded DOX were induced effective cancer cell death, and showed responses that were dependent on drug concentration and release

behavior (Figure 6). At lower DOX concentrations (2.5 μg/ml, and 5 μg/ml), better cell killing efficiency was achieved at quicker drug release conditions. Following the increase of DOX concentration, more complex cell killing behaviors appeared in our systems. Although cytotoxicity usually improved following increased drug concentration, the various drug release behaviors of the microspheres resulted in significantly different cell viabilities at the same DOX concentration, even achieving better cell killing efficiency at lower DOX concentrations. For example, when the DOX concentration was 10 μg/mL, the best cytotoxicity to cancer cells appeared with the M-300 microspheres, which was also better than that of the M-300, M-305, and M-310 samples with DOX concentrations of 20 μg/mL. This was also better than that with M-300 and M-305 with DOX concentrations of 40 μg/mL. The results suggested that both DOX amount and their release behaviors could significantly affect the cell death behavior, which also was worth studying in future. Confocal fluorescence images of co-stained cells also confirmed the dependence of cell killing capacity on drug release behavior (Figure 7), and revealed that the DOX released from DOX-loaded microspheres enter cells (Figure 6). While there was no direct evidence that the DOX-loaded microspheres entered the cells by endocytosis, the results suggested that improved therapeutic efficacy could be achieved at lower drug doses by tuning drug release behavior, a challenge for previous DDS systems[47–51].

Therefore, the present vaterite microsphere DDS system provides a simple but effective way to optimize anticancer effects. The microspheres still have drawbacks such as poor water dispersibility due to the micrometer scale size. However, with further optimization these issues could be addressed.

Conclusions

A silk-vaterite DDS system that can actively control drug release behavior was demonstrated. The silk content was tuned via a relatively simple thermal treatment to regulate the stability of vaterite microspheres, which then resulted in the controlled release of loaded drugs. More complex drug release behaviors could be designed through adjusting the ratios of various thermal-treated silk-vaterite microspheres. Cell viability results demonstrated different cytotoxicity efficacies of the microspheres towards cancer cells under same drug concentration but various release behaviors, suggesting the possibility of achieving desirable lower drug doses. Therefore, our present study provides a novel way to design vaterite-based carriers with tunable sustained release behaviors.

Supplementary Material

Refer to Web version on PubMed Central for supplementary material.

Acknowledgements

We thank National Basic Research Program of China (973 Program, 2013CB934400), NSFC (21174097, 51403144) and the NIH (R01 DE017207). We also thank the Priority Academic Program Development of Jiangsu Higher Education Institutions (PAPD), and the Excellent Youth Foundation of Jiangsu Province (BK2012009) for support of this work, and the Natural Science Foundation of Jiangsu Province (BK20140401).

References

1. Carelle N, Piotto E, Bellanger A, Germanaud J, Thuillier A, Khayat D. Cancer. 2000; 95:155. [PubMed: 12115329]
2. Glynne-Jones R, Grainger J, Harrison M, Ostler P, Makris A. Br. J. Cancer. 2006; 94:363. [PubMed: 16465172]
3. Peer D, Karp JM, Hong S, FaroKhzad OC, Margalit R, Langer R. Nat. Nanotechnol. 2007; 2:751. [PubMed: 18654426]
4. Danhier F, Feron O, Preat V. J Controlled Release. 2010; 148:135.
5. Basit AW. Drugs. 2005; 65:1991. [PubMed: 16162022]
6. Braun K, Pipkorn R, Waldeck W. Curr. Med. Chem. 2005; 12:1841. [PubMed: 16101505]
7. Phillips KA, Veenstra DL, Sadee W. Health Serv. Res. 2000; 35:128. [PubMed: 16148957]
8. Muvaffak A, Gurhan I, Gunduz U. J Drug Targeting. 2005; 13:151.
9. Endo T, Nakagawa T, Kita T, Kim TS, Iguchi F, Naito Y, Tabata Y, Ito J. Otolaryng. Head Neck. 2004; 131:260.
10. Li DC, Zhong XK, Zeng ZP, Jiang JG, Li L, Zhao MM, Yang XQ, Chen J, Zhang BS, Zhao QZ. J Controlled Release. 2009; 138:103.
11. Germershaus O, Werner V, Kutscher M, Meinel L. Biomaterials. 2014; 35:3427. [PubMed: 24461326]
12. Riehemann K, Schneider SW, Luger TA, Godin B, Ferrari M, Fuchs H. Angew. Chem. Int. Ed. 2009; 48:872.
13. Kim C, Agasti SS, Zhu ZJ, Isaacs L, Rotello VM. Nat. Chem. 2010; 2:962. [PubMed: 20966953]
14. Park JH, Saravanakumar G, Kim K, Kwon IC. Adv. Drug Delivery Rev. 2010; 62:28.
15. Ahmed F, Discher DE. J Controlled Release. 2004; 96:37.
16. Ge H, Hu Y, Jiang X, Cheng D, Yuan Y, Bi H, Yang C. J Pharm. Sci. 2002; 91:1463. [PubMed: 12115846]
17. Gajbhiye V, Jain NK. Biomaterials. 2011; 32:6213. [PubMed: 21616528]
18. Li X, Qian Y, Liu T, Hu X, Zhang G, You Y, Liu S. Biomaterials. 2011; 32:6595. [PubMed: 21663960]
19. Cui W, Cui Y, Zhao J, Li J. J Mater. Chem. B. 2013; 1:1326.
20. Jiang SP. J Mater. Chem. A. 2014; 2:7637.
21. Guo YP, Guo LH, Yao YB, Ning CQ, Guo YJ. Chem. Commun. 2011; 47:12215.
22. Kim S, Park CB. Adv. Funct. Mater. 2013; 23:10.
23. Zhang Q, Liu F, Nguyen KT, Ma X, Wang X, Xing B, Zhao Y. Adv. Funct. Mater. 2012; 22:5144.
24. De Smet R, Verschuere S, Allais L, Leclercq G, Dierendonck M, De Geest BG, Van Driessche I, Demoor T, Cuvelier CA. Biomacromolecules. 2014; 15:2301. [PubMed: 24805802]
25. Lauth V, Maas M, Rezwan K. J Mater. Chem. 2014; B2:7725.
26. Zhao Y, Lu Y, Hu Y, Li JP, Dong LA, Lin LN, Yu SH. Small. 2010; 6:2436. [PubMed: 20878636]
27. Ma MY, Zhu YJ, Li L, Cao SW. J Mater. Chem. 2008; 18:2722.
28. Wei W, Ma GH, Hu G, Yu D, McLeish T, Su ZG, Shen ZY. J Am. Chem. Soc. 2008; 130:15808. [PubMed: 18980322]
29. Wang J, Chen JS, Zong JY, Zhao D, Li F, Zhuo RX, Cheng SX. J Phys. Chem. C. 2010; 114:18940.
30. Zhao Y, Lin LN, Lu Y, Chen SF, Dong LA, Yu SH. Adv. Mater. 2010; 22:5255. [PubMed: 20972977]
31. Ueno Y, Futagawa H, Takagi Y, Ueno A, Mizushima Y. J Controlled Release. 2005; 103:93.
32. Wang C, Liu H, Gao Q, Liu X, Tong Z. Carbohydr. Polym. 2008; 71:476.
33. Wang C, He C, Tong Z, Liu X, Ren B, Zeng F. Int. J. Pharm. 2006; 308:160. [PubMed: 16359836]
34. Kurapati R, Raichur AM. J Mater. Chem. B. 2013; 1:3175.
35. Guo Y, Zhang J, Jiang L, Shi X, Yang L, Fang Q, Fang H, Wang K, Jiang K. Chem. Commun. 2012; 48:10636.

36. Peng H, Li K, Wang T, Wang J, Wang J, Zhu R, Sun D, Wang S. Nanoscale Res. Lett. 2013; 8:1. [PubMed: 23279756]
37. Wei J, Cheang T, Tang B, Xia H, Xing Z, Chen Z, Fang Y, Chen W, Xu A, Wang S, Luo J. Biomaterials. 2013; 34:1246. [PubMed: 23127333]
38. Luo R, Venkatraman SS, Neu B. Biomacromolecules. 2013; 14:2262. [PubMed: 23692337]
39. Ferrari M. Nat. Rev. Cancer. 2005; 5:161. [PubMed: 15738981]
40. Huang X, Brazel CS. J Controlled Release. 2001; 73:121.
41. Couvreur P. Adv. Drug Delivery Rev. 2013; 65:21.
42. Cheng C, Shao Z, Vollrath F. Adv. Funct. Mater. 2008; 18:2172.
43. Wang T, Porter D, Shao Z. Adv. Funct. Mater. 2012; 22:435.
44. Wang T, Che R, Li W, Mi R, Shao Z. Cryst. Growth Des. 2011; 11:2164.
45. Liu L, Zhang X, Liu X, Liu J, Lu G, Kaplan DL, Zhu H, Lu Q. ACS Appl. Mater. Interfaces. 2015; 7:1735. [PubMed: 25578091]
46. Kabalah-Amitai L, Mayzel B, Kauffmann Y, Fitch AN, Bloch L, Gilbert PU, Pokroy B. Science. 2013; 340:454. [PubMed: 23620047]
47. Mugnaioli E, Andrusenko I, Schüler T, Loges N, Dinnebier RE, Panthöfer M, Tremel W, Kolb U. Angew. Chem. Int. Ed. 2012; 51:7041.
48. Parakhonskiy BV, Haase A, Antolini R. Angew. Chem. Int. Ed. 2012; 51:1195.
49. Forsgren J, Andersson M, Nilsson P, Mihranyan A. Adv. Healthcare Mater. 2013; 2:1469.
50. Svenskaya Y, Parakhonskiy B, Haase A, Atkin V, Lukyanets E, Gorin D, Antolini R. Biophys. Chem. 2013; 182:11. [PubMed: 23932207]
51. Serajuddin ATM. J Pharm. Sci. 1999; 88:1058. [PubMed: 10514356]
52. Rockwood DN, Preda RC, Yücel T, Wang X, Lovett ML, Kaplan DL. Nat. Protoc. 2011; 6:1612. [PubMed: 21959241]
53. Lu Q, Zhu H, Zhang C, Zhang F, Zhang B, Kaplan DL. Biomacromolecules. 2012; 13:826. [PubMed: 22320432]
54. Wolf G, Günther C. J Therm. Anal. Calorim. 2001; 65:687.
55. Sui C, Lu Y, Gao HL, Dong L, Zhao Y, Ouali L, Benczedi D, Jerri H, Yu S. Cryst. Growth Des. 2013; 13:3201.

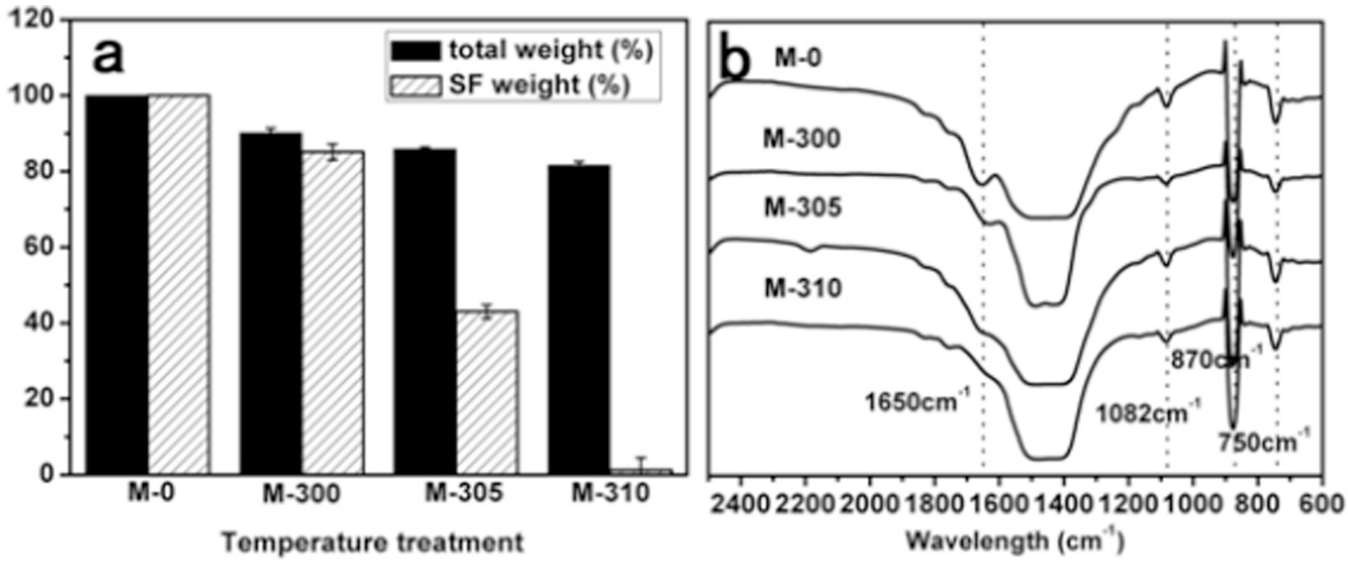

Figure 1.

The weight and structural changes of the silk-vaterite microspheres after different thermal treatments: (a) The weight loss of the microspheres after thermal treatment when compared with the control (M-0). The original silk content inside the microspheres before thermal treatment was 10%, based on TGA curves of the particles from 0 to 800°C at 10 °C min^{-1} in a nitrogen gas with flow rate of 40 $cm^3 min^{-1}$ (The curves are not shown). (b) FTIR spectra of the $CaCO_3$ microspheres after different thermal treatments. The typical peaks of silk gradually decreased and almost disappeared following the increase of temperature and time while the peaks of vaterite keep stable in the processes.

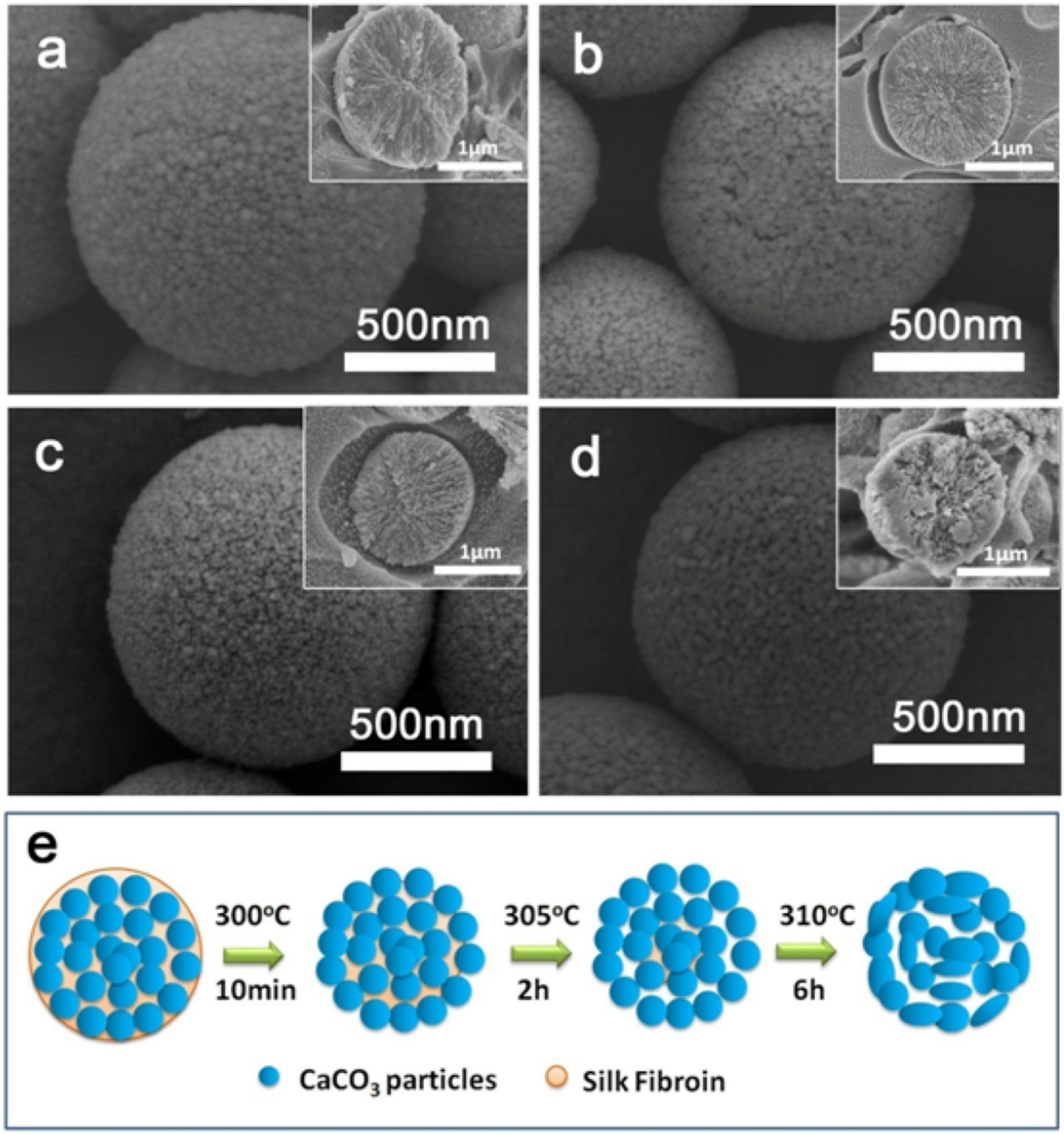

Figure 2.

SEM images of silk-vaterite microspheres after different thermal treatments: (a) M-0; (b) M-300; (c) M-305; and (d) M-310; (e) Schematic diagram of the morphology changes for the silk-vaterite microspheres after different thermal treatments. The microspheres with size of 1–2 μm were composed of vaterite nanoparticles with diameter of tens of nanometers that could fuse following the removal of the silk. The inserts in (a–d) are cross-section images.

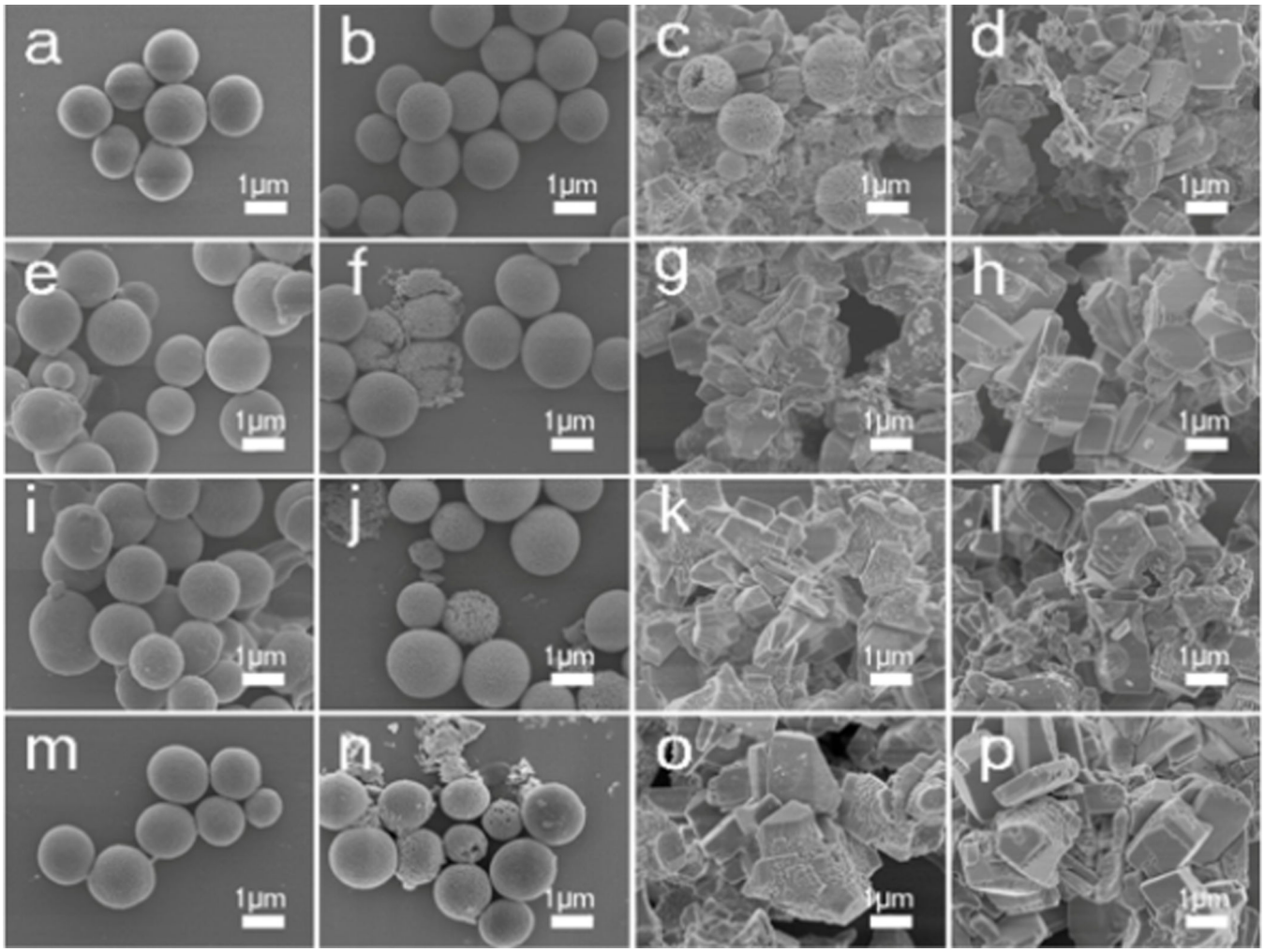

Figure 3.

Morphology changes of the thermal treated vaterite microspheres when incubated in a flowing water: (a, e, i, m) M-0; (b, f, j, n) M-300; (c, g, k, o) M-305; and (d, h, l, p) M-310. The incubation times for the samples were as follows: (a, b, c, d) 2 days; (e, f, g, h) 4 days; (I, j, k, l) 6 days; and (m, n, o, p) 8days. More rapid vaterite-calcite transitions occurred following the decrease of silk content inside the microspheres.

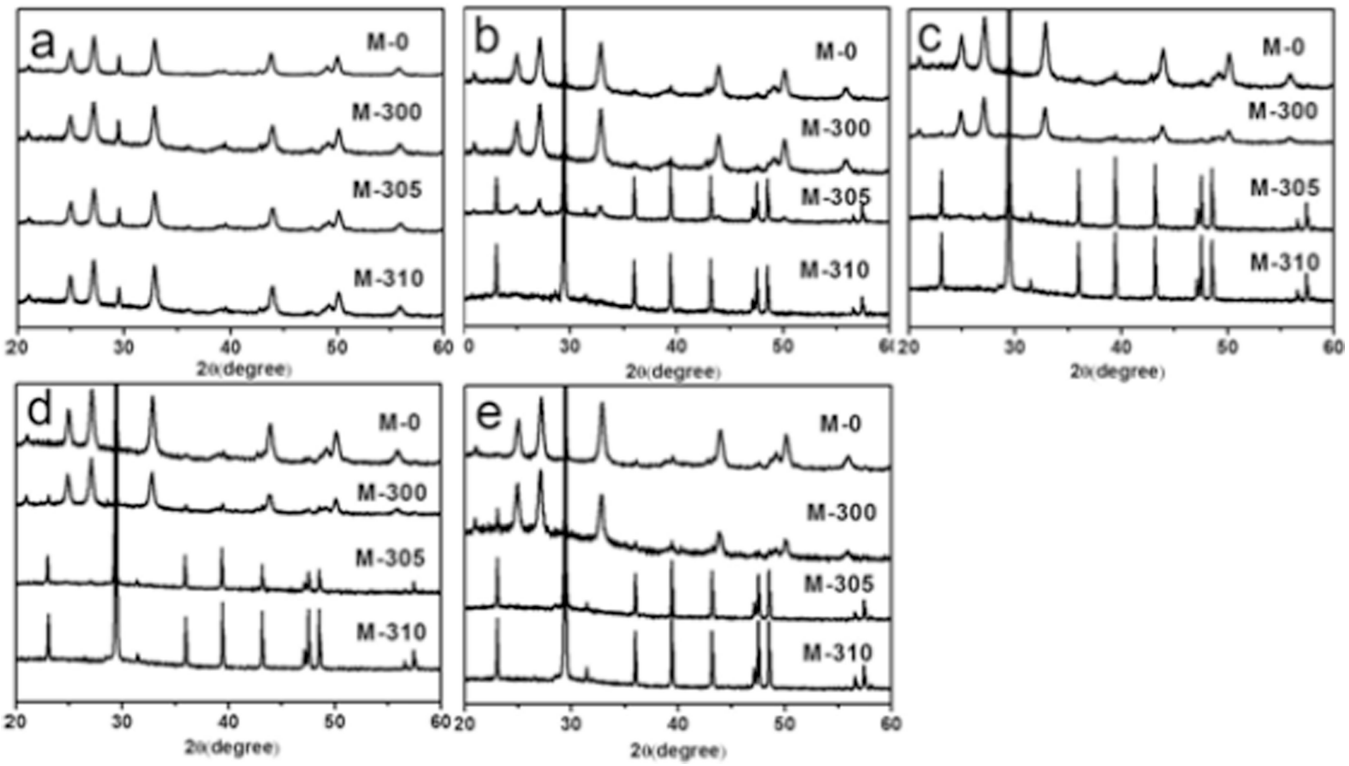

Figure 4.

Polymorph changes of the thermal-treated vaterite microspheres when incubated in flowing water: (a) 0 days, (b) 2 days, (c) 4 days, (d) 6 days, and (e) 8 days. More rapid vaterite-calcite transitions appeared following the decrease of silk content inside the microspheres.

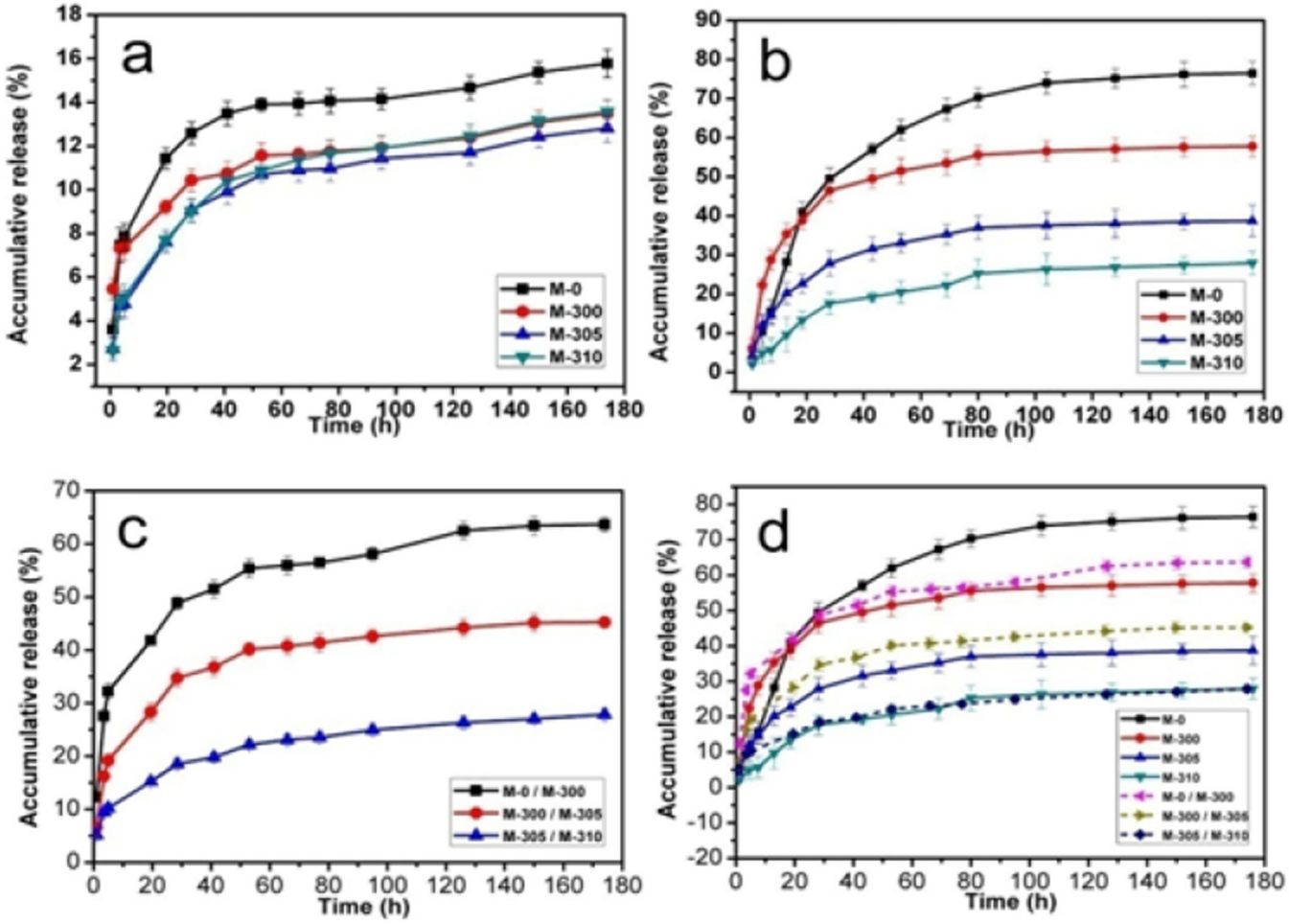

Figure 5.

DOX release behavior from the thermal treated silk-vaterite microspheres: (a) pH= 7.4, (b) pH= 4.5, (c) the drug release behaviors from blend silk-vaterite microspheres at pH of 4.5 and (d) the total drug release behaviors from different microsphere systems at pH of 4.5. The samples were as follows: M-0, DOX-loaded M-0 microspheres; M-300, DOX-loaded M-300 microspheres; M-305, DOX-loaded M-305 microspheres; M-310, DOX-loaded M-310 microspheres; M-0/M-300, DOX-loaded blend microspheres composed of M-0 and M-300 at weight ratio of 1:1; M-300/M-305, DOX-loaded blend microspheres composed of M-300 and M-305 at weight ratio of 1:1; and M-305/M-310, DOX-loaded blend microspheres composed of M-305 and M-310 at weight ratio of 1:1. All the release measurements were repeated in triplicate.

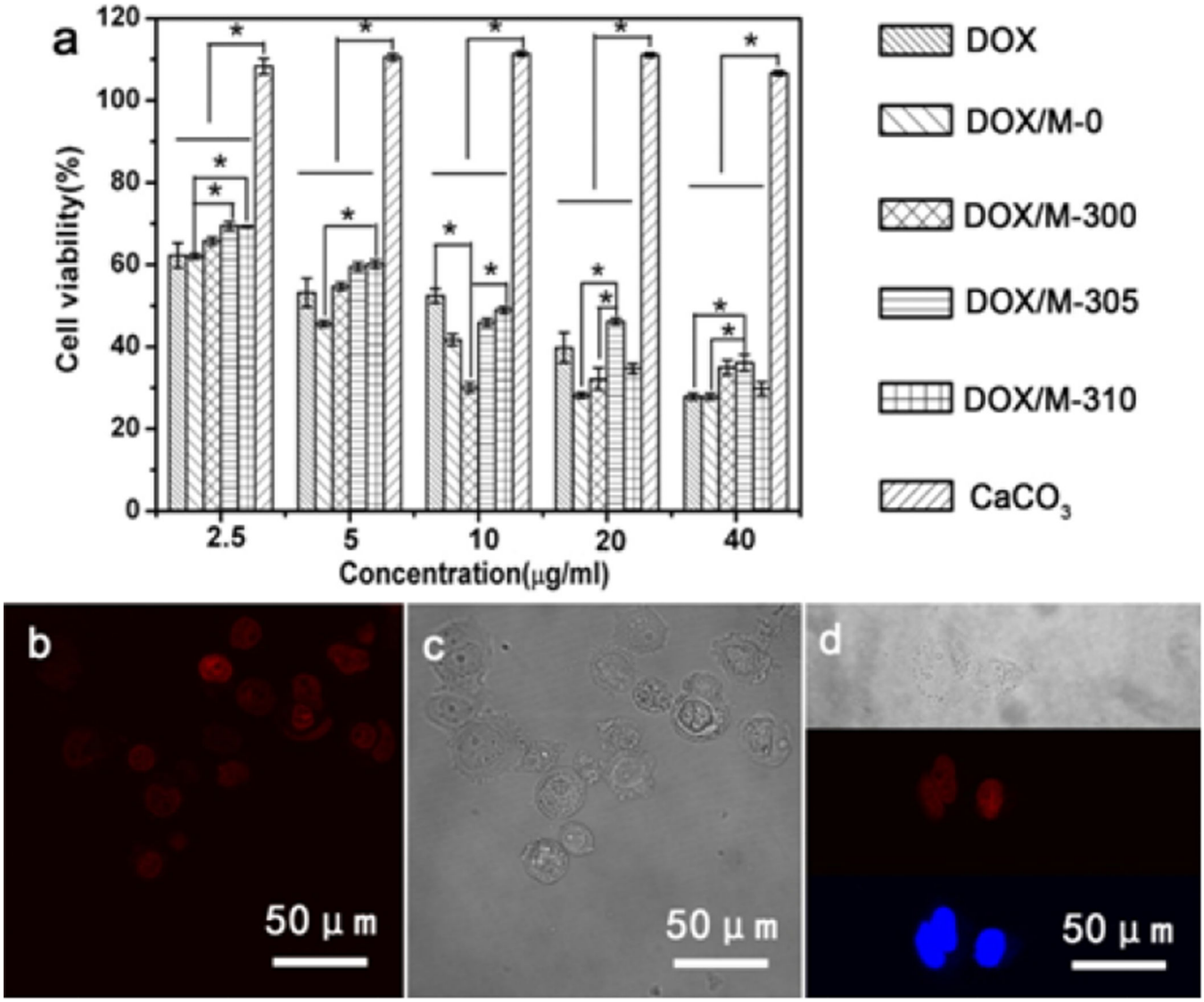

Figure 6.

The cytotoxicity efficacy of DOX-loaded silk-vaterite microspheres on MDA-MB-231 cells cultured for 5 days: (a) CCK-8 assay of MDA-MB-231 cells under different DOX concentrations. The samples were as follows: DOX, free DOX; DOX/M-0, DOX-loaded M-0; DOX/M-300, DOX-loaded M-300; DOX/M-305, DOX-loaded M-305; DOX/M-310, DOX-loaded M-310; and $CaCO_3$, various DOX-free silk-vaterite microspheres; (b–d) Confocal fluorescence images of MDA-MB-231 cells when cultured with DOX-loaded M-300 microspheres at DOX concentration of 10 μg/mL for 5 days. The blue stands for DAPI, the red stands for DOX. The images indicate that DOX released from DOX-loaded microspheres enter cells.

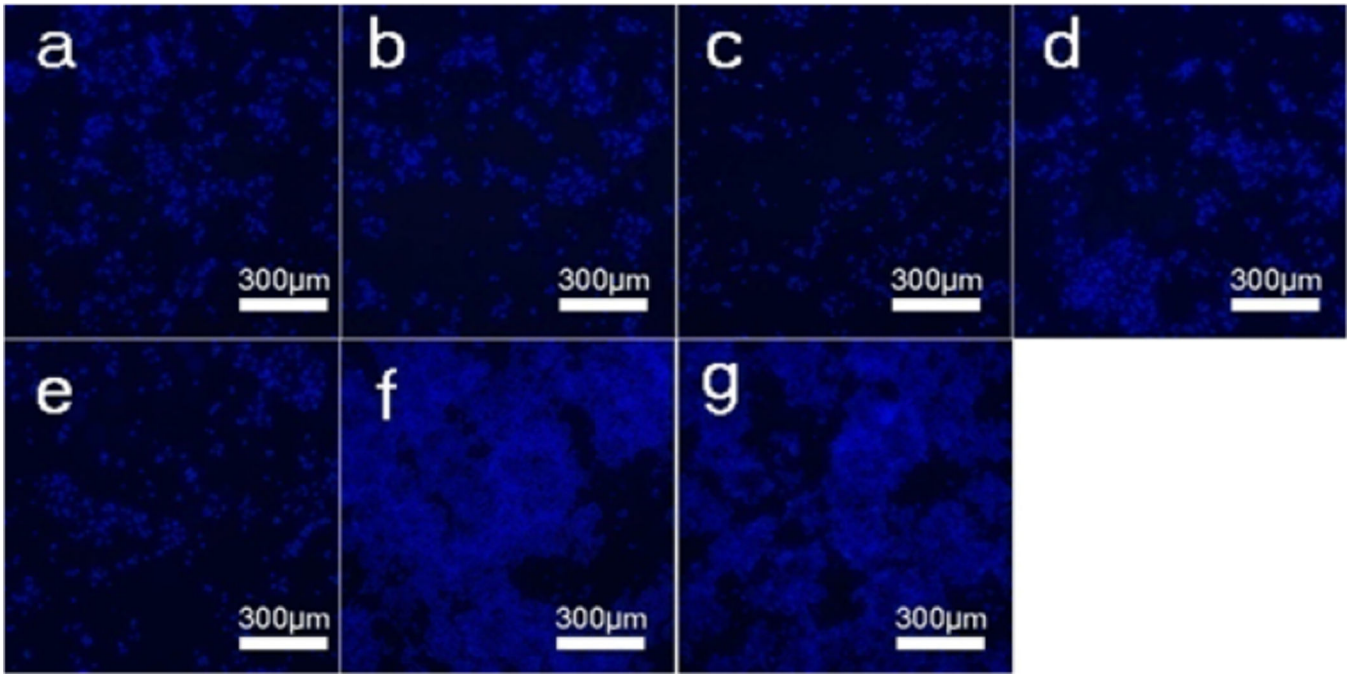

Figure 7.

Confocal fluorescence images of MDA-MB-231 breast cancer cells after incubation with different DOX-loaded microspheres at a DOX concentration of 10 μg/mL for 5 days. The samples were as follows: (a) DOX-loaded M-0, (b) DOX-loaded M-300, (c) DOX-loaded M-305, (d) DOX-loaded M-310, (e) Free DOX, (f) DOX-free vaterite microspheres (M-0), and (g) blank plate as control. The blue (DAPI) is living cancer cells.

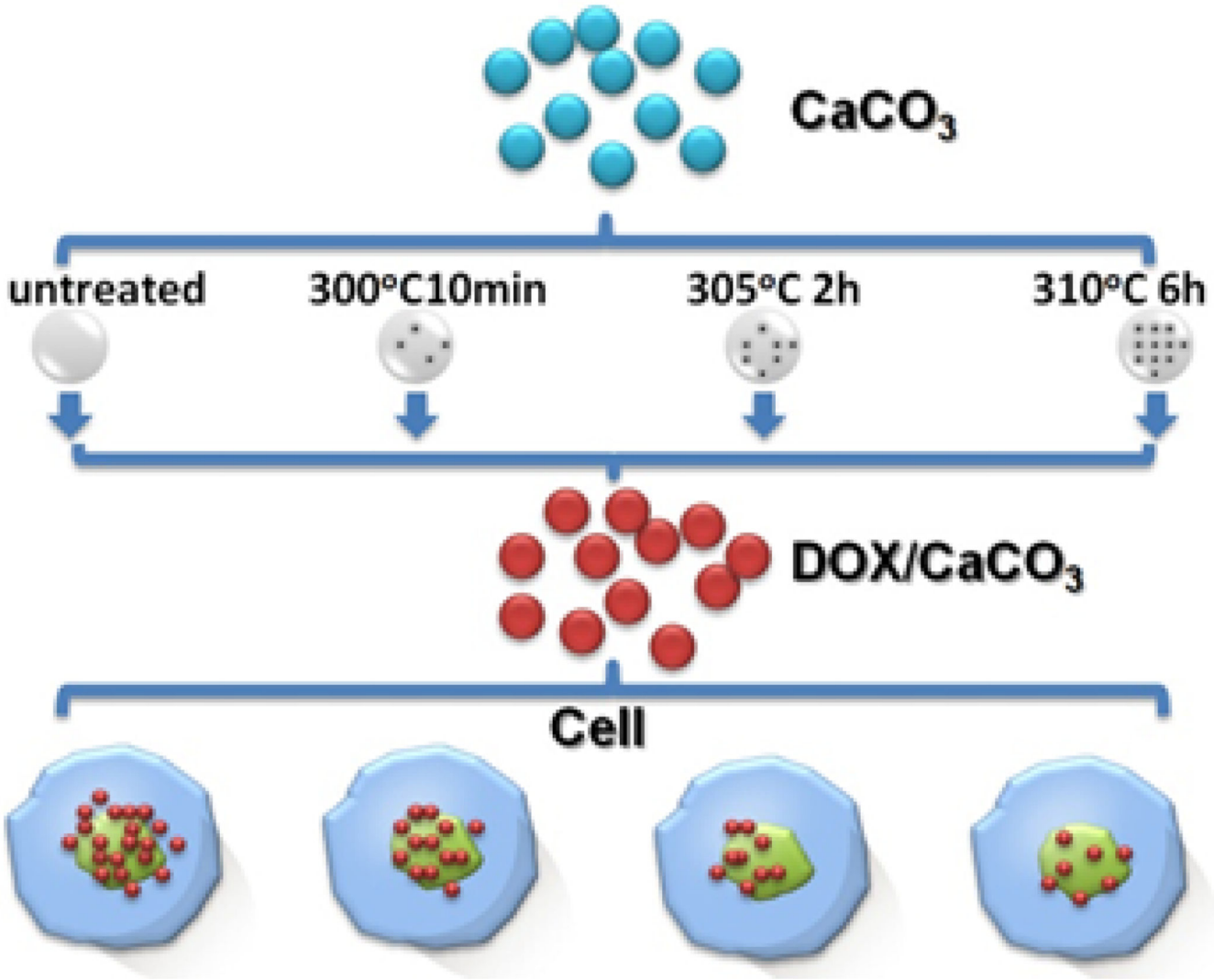

Scheme 1.
The strategy for the preparation of silk-vaterite microspheres with tunable release behaviors through thermal treatment processes.

Table 1

DOX-loading properties of the thermal treated vaterite microspheres

Samples	M-0	M-300	M-305	M-310
Entrapment efficiency (%)	93.1±1.8	92.4±3.2	94.4±2.4	94.2±2.9
Drug loading content (%)	4.66±0.09	4.62±0.16	4.72±0.12	4.71±0.15